Enhanced antineutrino emission from β decay in core-collapse supernovae with self-consistent weak decay rates

T. Dasher 0, 1, 2, * A. Ravlić $0, 1, 3, \dagger$ S. Lalit $0, 1, \ddagger$ E. O'Connor $0, 4, \S$ and K. Godbey $0^{1}, \P$

¹Facility for Rare Isotope Beams, Michigan State University, East Lansing, Michigan 48824, USA
²Department of Physics and Astronomy, Michigan State University, East Lansing, Michigan 48824, USA
³Department of Physics, Faculty of Science, University of Zagreb, Bijenička c. 32, 10000 Zagreb, Croatia

⁴The Oskar Klein Centre, Department of Astronomy,
Stockholm University, AlbaNova, SE-106 91 Stockholm, Sweden
(Dated: November 27, 2025)

Nuclear weak-interaction rates are known to exert a prominent effect in the late-stages of stellar collapse. Despite their importance, most studies to date on core-collapse supernovae (CCSNe) have focused primarily on the effects of electron captures, generally neglecting β decay contributions. In this Letter, we present the first CCSNe simulation incorporating global β decay rates from a microscopic theory. These are enabled by a large-scale evaluation of both electron capture and β decay rates, obtained self-consistently utilizing the relativistic energy density functional theory and finite-temperature quasiparticle random-phase approximation. We find a significant enhancement of antineutrino emissivity by more than 4 orders of magnitude due to the inclusion of β decay rates, as well as 3 orders of magnitude for antineutrino luminosity. It is expected that these new rates could help us constrain the model uncertainties related to weak-interaction processes, improving the prediction of antineutrino signal during the final stages of stellar death and potentially influencing the late-stage evolution of massive stars.

Introduction.— The detection of a total of 25 events in the neutrino burst of supernova 1987A [1-3] has led to several improvements in the detection techniques of the Earth-based neutrino observatories [4–8] as well as global network for supernova early warning systems [9– 11] integrating presupernova antineutrino $(\bar{\nu}_e)$ detection. Weak interactions play a central role in the final stages of stellar evolution, where stellar interiors are characterized by high temperatures and densities [12–16]. One of the most prominent processes during the early collapse phase of core-collapse supernovae (CCSNe) is electron capture (EC), with rates increasing rapidly at higher temperatures and densities. In contrast, due to blocking of the lepton phase-space, β decay rates decrease considerably at higher densities. Nevertheless, during a brief but important interval in the presupernova phase, EC and β decay can compete [17]. At presupernova-like conditions, both EC and β decays are dominated by allowed Fermi and Gamow-Teller (GT) transitions with nuclear composition consisting mostly of pf-shell nuclei [18]. However, as the collapse proceeds, the contribution of forbidden transitions and heavier nuclei becomes nonnegligible. EC and β decay rates were initially estimated in Refs. [19–22] using the independent particle model with a single GT resonance, and supplemented, where available, by experimental data for low-lying transitions. Later, these rates were calculated using the nuclear shellmodel (SM) up to A = 40 [23] and for A = 45-65 [24-26]. Impact of β decay rates on presupernova (anti)neutrinos, based on SM calculations for pf-shell nuclei, was investigated in Refs. [27–30], revealing a substantial effect on the subsequent stellar evolution. While nuclei in the vicinity of ⁵⁶Fe dominate the presupernova composition,

heavier nuclei (A > 60) increasingly contribute as the collapse proceeds [14]. However, SM calculations quickly become numerically infeasible for these nuclei due to prohibitive scaling with the system size. The approaches based on the energy density functional (EDF) theory, in principle, allow for extending calculations of weakinteraction processes throughout the nuclide chart, and also include more complicated forbidden transitions. Excited states can be efficiently probed employing the quasiparticle random-phase approximation (QRPA), with the residual interaction derived self-consistently from the underlying EDF [31]. This approach also allows for inclusion of finite-temperature effects within the finitetemperature QRPA (FT-QRPA) [32, 33]. In particular, recent calculations involving consistent treatment of GT transitions in hot nuclei, within the thermal QRPA, predicted enhancement of the energy luminosity and average energies in ⁵⁶Fe of the emitted (anti)neutrinos [34–37]. In this Letter, following the recent work on EC in Ref. [38], we perform large-scale calculations of β decay rates obtained within the EDF+FT-QRPA framework and study its impact on the CCSNe evolution.

Methods.—The theoretical framework employed for calculating the β decay rates is based on the relativistic EDF theory with the momentum-dependent D3C* interaction [39–41], computational framework being detailed in Refs. [39, 42]. The initial nuclear states are determined by the finite-temperature Hartree-Bardeen-Cooper-Schrieffer (FT-HBCS) theory assuming spherical symmetry [33, 43], while the final states and transition strengths are determined within the FT-QRPA [33, 44, 45]. Crucially, for β decays we carefully consider the contribution of de-excitations from highly-excited

states in the parent nucleus [42]. Apart from the allowed GT transitions, we also consider the first-forbidden (FF), $J^{\pi} = 0^{-}$, 1^{-} and 2^{-} , transitions that contribute to the β decay rate for neutron-rich nuclei. Nuclei are assumed to be fully ionized with electrons(positrons) in the plasma described by the Fermi-Dirac distribution, meaning that β decay rates are a function of the temperature T and a product of stellar density with the electron-to-baryon ratio ρY_e . The β decay rates can be expressed through the electron antineutrino spectral functions $n(E_{\bar{\nu}_e})$, summed over all the contributing multipoles J^{π} [46]

$$\lambda_{\beta}^{(i)} = \sum_{J^{\pi}} \int_{0}^{Q_{\beta}} n_{i}(E_{\bar{\nu}_{e}}, J^{\pi}) dE_{\bar{\nu}_{e}}, \tag{1}$$

along with the antineutrino energy loss rate

$$\lambda_{\bar{\nu}_e}^{(i)} = \sum_{J^{\pi}} \int_{0}^{Q_{\beta}} E_{\bar{\nu}_e} n_i(E_{\bar{\nu}_e}, J^{\pi}) dE_{\bar{\nu}_e}, \tag{2}$$

where $E_{\bar{\nu}_e}$ is the electron antineutrino energy, and Q_{β} is the β decay energy window.

Model calculations include a large set of β decay rates consisting of a total of 902 individual nuclei from the proton to the neutron drip line, and from calcium (Z=20) to zirconium (Z=40). The considered temperatures span a range from 1 to 30 GK, with a respective range in densities from $\rho Y_e=10^5$ to 10^{12} g/cm³, enough to consider the CCSNe trajectories where β decays are of relevance. The β decay table includes a set of $(\lambda_{\beta}, \lambda_{\bar{\nu}_e})$ values at specific $(T, \rho Y_e)$ conditions. We evaluate the antineutrino spectral function as

$$n_i(E_{\bar{\nu}_e}) = \mathcal{N}_i E_{\bar{\nu}_e}^2 (E_{\bar{\nu}_e} - q_i)^2 \frac{e^{(E_{\bar{\nu}_e} - \mu_e - q_i)/T}}{1 + e^{(E_{\bar{\nu}_e} - \mu_e - q_i)/T}} \Theta(q_i - E_{\bar{\nu}_e}),$$
(3)

with effective Q-value, q_i , determined by reproducing the average antineutrino energy $\langle E_{\bar{\nu}_e} \rangle = \lambda_{\bar{\nu}_e} / \lambda_{\beta}$, and \mathcal{N}_i the overall normalization constant. The differential antineutrino emissivity, henceforth antineutrino emissivity, is subsequently given by

$$\frac{d\epsilon_{\bar{\nu}_e}}{d\Omega dE_{\bar{\nu}_e}} = \sum_i \frac{E_{\bar{\nu}_e}}{4\pi} Y_i n_i(E_{\bar{\nu}_e}), \tag{4}$$

where the summation is performed over all nuclei whose abundance Y_i is given by the nuclear statistical equilibrium (NSE) composition. Employing our rates, the emissivities are calculated using the open-source neutrino library NuLib [48]. While we focus on β decay rates, we employ the EC rates from a recent work (see Ref. [38]), obtained within the same theoretical framework. To study the impact of new β decay rates on antineutrino emissivity, we examine the results obtained with three models. In the first case, we neglect the contribution

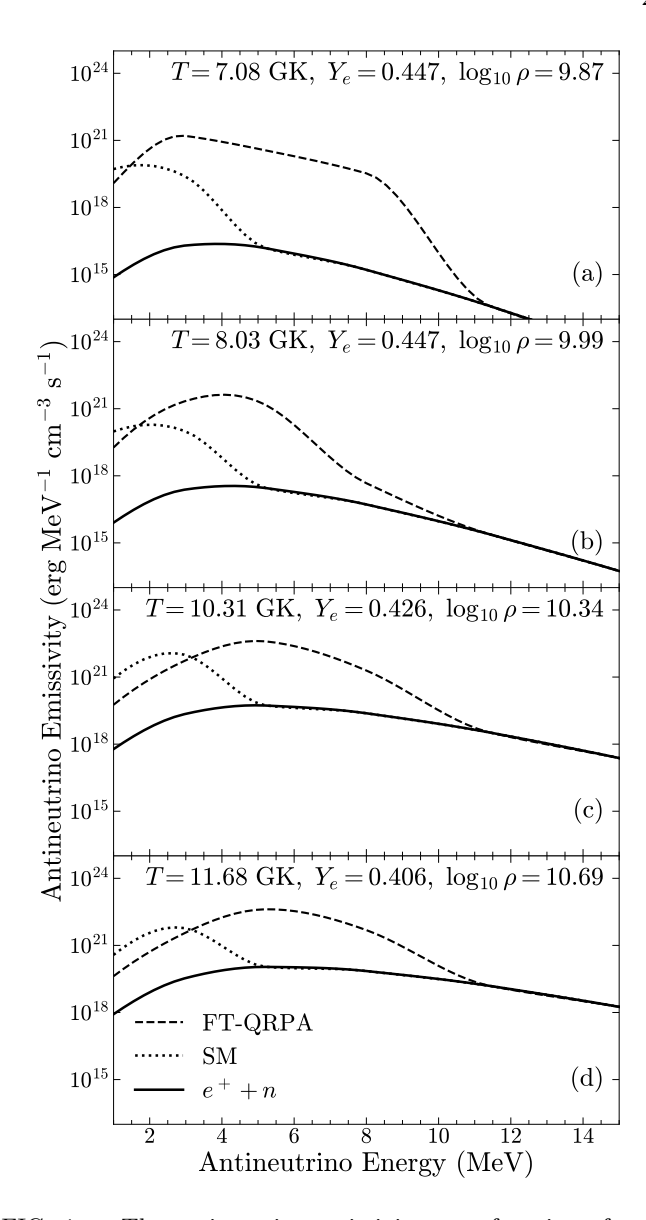


FIG. 1. The antineutrino emissivity as a function of antineutrino energy at 4 sets of thermodynamic conditions during the CCSNe evolution of a $20M_{\odot}$ progenitor (a)–(d). The positron capture on free neutrons, $e^+ + n$, contribution (solid line), as a baseline in all models, is compared to emissivities where the β decay rates are explicitly included either from the FT-QRPA calculations in this work (dashed line) or the shell-model data (dotted line) [26, 47].

of β decays and only consider the positron capture on free neutrons $e^+ + n \to p + \bar{\nu}_e$, with formalism described in NuLib documentation [48]. For models that consider β decays, we utilize our calculations (labeled FT-QRPA in the following) or SM calculations from Refs. [26, 47], mostly in the pf-shell region. The nuclear composition is determined by the SFHo equation of state [49]. The CCSNe simulation is performed using the open-source code GR1D [48] solving for early and post-bounce stages in spherical symmetry with general relativistic hydro-

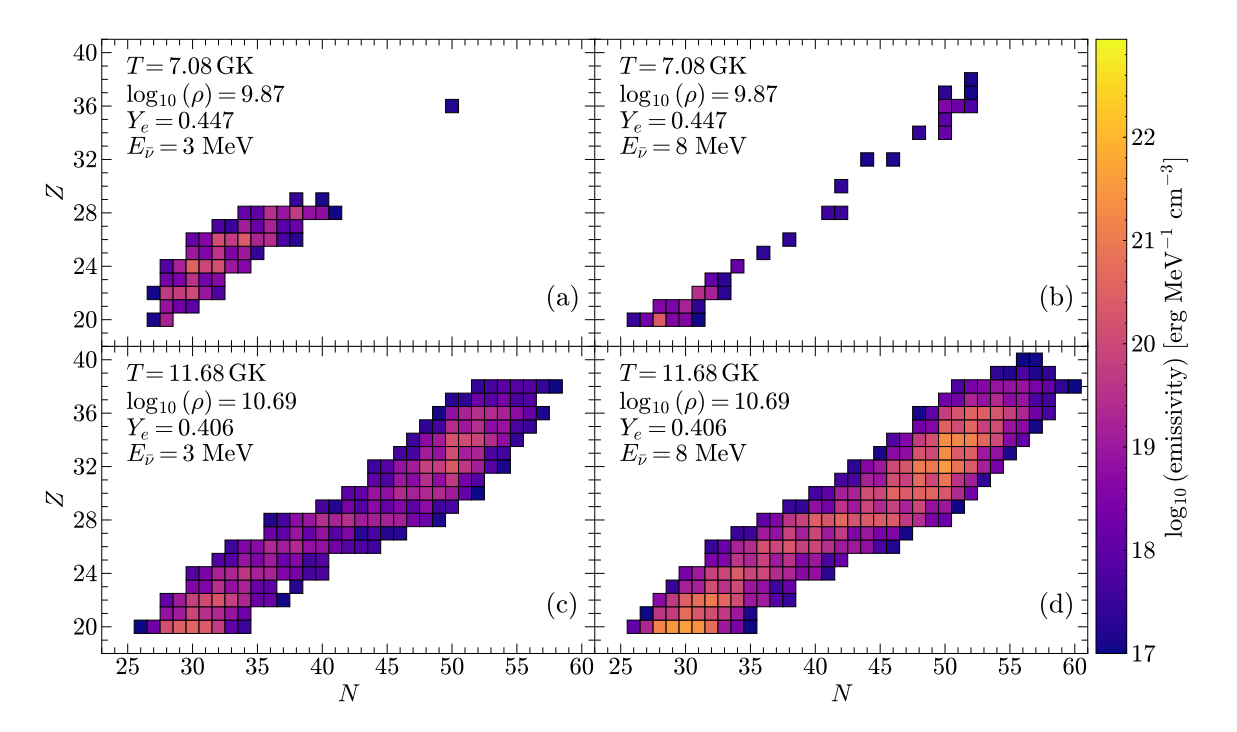


FIG. 2. Partial contribution of individual nuclei to the total antineutrino emissivity at $E_{\bar{\nu}_e} = 3$ MeV (a,c) and $E_{\bar{\nu}_e} = 8$ MeV (b,d) at conditions corresponding to the onset of the collapse (a,b) and closer to the time of the bounce (c,d). All rates are obtained with the FT-QRPA model.

dynamics. All simulations performed in this work consider either a $15M_{\odot}$ or $20M_{\odot}$ solar-metallicity progenitor (s15WW95, s20WW95) [50].

Results.— Results for the antineutrino emissivity [cf. Eq. (4)] are shown in Fig. 1 (panels (a)-(d)) across four representative points on the CCSNe thermodynamic trajectory of a $20M_{\odot}$ progenitor. Emissivities obtained using three different models are compared. Our baseline model, labeled $e^+ + n$, includes only positron capture on free neutrons, excluding nuclear β decays. For the models containing nuclear β decay, one model uses the FT-QRPA rates for 902 nuclei calculated herein, and the other uses SM rates from Refs. [26, 47]. Starting from the onset of the collapse in Fig. 1(a), we observe a huge enhancement of antineutrino emissivities due to inclusion of β decays, relative to the baseline model. The FT-QRPA calculation yields an increase of nearly four orders of magnitude, peaking around $E_{\bar{\nu}_e} \approx 3$ MeV and extending up to ≈ 11 MeV. For the SM rates, there is a somewhat lower enhancement, peaked at a lower $E_{\bar{\nu}_e}$, and converging rapidly to the positron capture baseline for $E_{\bar{\nu}_e} \approx 5$ MeV. The β decay is constrained by the Q_{β} energy window [cf. Eq. (1)]. This window measures approximately 11 MeV for neutron-rich nuclei but is significantly lower for pf-shell nuclei. We note that the SM rates are available for nuclei up to A < 65, which can only span a limited range in the Q_{β} values. On average, as was remarked in Ref. [38], the FT-QRPA rates

are higher than those predicted by the SM (check Figs. S2 and S3 in the Supplemental Material [51]). This difference is attributable to multiple factors, such as the inclusion of first-forbidden transitions and the consistent treatment of de-excitations within the FT-QRPA. With increasing temperature, β decay rates tend to increase, while with increasing density, the rates are significantly hindered [45]. We notice that with increasing temperature and density in Fig. 1(b)–(d) both FT-QRPA and SM emissivities stay approximately the same, with the peaks shifting to larger $E_{\bar{\nu}_e}$, primarily due to β decay rates being blocked by increasing density, while the contribution of positron capture on neutrons antineutrino baseline increases. Therefore, there is a window, up to around $\log_{10} \rho Y_e \approx 10$, where β decay can produce a significant number of antineutrinos.

To study in greater detail which nuclei contribute the most to enhanced emissivity due to inclusion of β decays, in Fig. 2, we show a partial emissivity for individual nuclei, by restricting Eq. (4) to a specific nucleus i. Results are shown as obtained with the FT-QRPA β decay rates. Based on the conclusions from Fig. 1 we focus on two antineutrino energies, $E_{\bar{\nu}_e}=3$ MeV and $E_{\bar{\nu}_e}=8$ MeV. Figure 2(a) identifies the nuclei primarily responsible for the emissivity peak observed in Fig. 1(a). Predictably, most of these nuclei are pf-shell. However, since the enhancement of the rates extends all the way to $E_{\bar{\nu}_e}\approx 8$ MeV, Fig. 2(b) displays the nuclei that con-

tribute most significantly to the emissivity at the same conditions, specifically constrained to $E_{\bar{\nu}_e} = 8$ MeV. As expected, we observe a more extended distribution of nuclei that contribute, even up to the N = 50 region, with larger Q_{β} values. Moving on, at higher temperatures and densities, closer to the conditions corresponding to those at the time of the core bounce, as seen in Fig. 1(d), a more extended distribution of nuclei contributes to the total emissivity. However, in Fig. 2(d), we can see two regions of the nuclide chart that display a more enhanced contribution to the emissivity located around (Z, N) = (20, 30), as well as the neutron-rich (Z, N) = (32, 50). An increase in $E_{\bar{\nu}_e}$ from 3 to 8 MeV enhances contribution of nuclei around N = 50 significantly as shown in Fig. 2. Therefore, predictive modeling of antineutrino spectra requires rate libraries that extend well into the medium-heavy mass region, such as those generated by our FT-QRPA calculations.

To study the impact of these rates, we implement them in CCSNe simulations using the EC rates from Ref. [38]. Panels (a) and (c) of Fig. 3 show the time evolution of the neutrino and antineutrino luminosity at 500 km from the core of $15M_{\odot}$ and $20M_{\odot}$ progenitors. The positron capture baseline antineutrino luminosity is shown by solid lines, while the dashed and dotted curves show the (anti)neutrino luminosity obtained using the FT-QRPA β decay rates. For the neutrino luminosity (dotted curves), the dominant component originates from the EC and shows exponential increase towards the bounce, which occurs at $t \approx 225 \text{ ms } (15M_{\odot})$ and $t \approx 300 \text{ ms } (20M_{\odot})$ after the onset of the collapse. The positron capture antineutrino luminosity exhibits a gradual increase up to the bounce. Once the β decays are accounted for, the antineutrino luminosity shows a considerable enhancement of more than 3 orders of magnitude compared to the $e^+ + n$ baseline. β decays bring the antineutrino luminosity closer to within 2 orders of magnitude of the neutrino one, for $20M_{\odot}$ progenitor. However, since the neutrino luminosity increases very steeply, as EC on heavier nuclei becomes temperatureunblocked, we observe no impact on CCSNe dynamics itself. Increased luminosity of antineutrinos enhances the antineutrino signal originating from β decays just prior to the bounce. To better showcase this, panels (b) and (d) in Fig. 3 display the time-evolution of the average (anti)neutrino energy. We observe that the antineutrino energy remains stable up to the bounce, as expected, considering the limited Q_{β} window and emissivity trends in Fig. 1. Similar trends are observed irrespective of the progenitor mass. Compared to the $e^+ + n$ baseline, the average antineutrino energy by including the FT-QRPA β decays increases, by around 0.4(0.5) MeV for $15M_{\odot}(20M_{\odot})$ progenitor, driven by the changes we observed in emissivity in Fig. 1. While the average antineutrino energy remains almost constant up to the bounce, the average electron neutrino energy continues to increase consider-

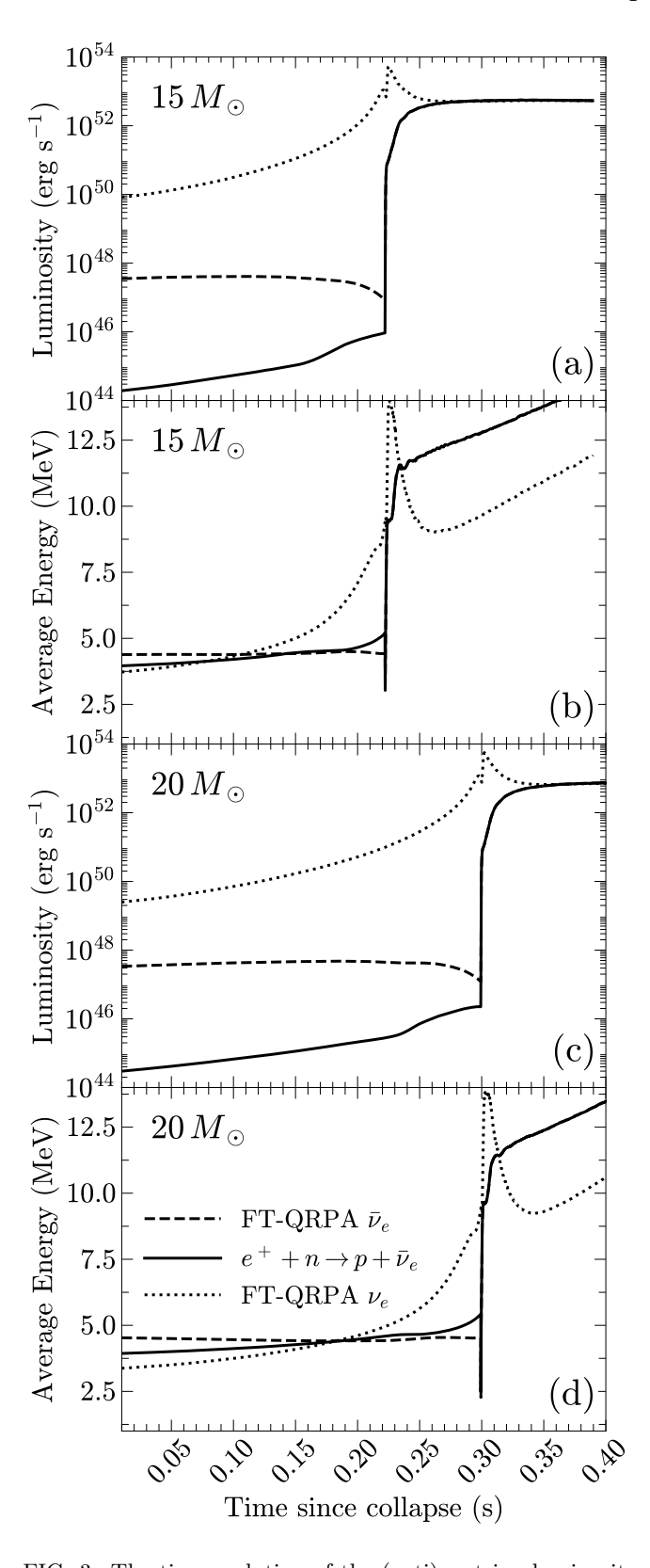


FIG. 3. The time-evolution of the (anti)neutrino luminosity at 500 km from the core (a,c) and the average (anti)neutrino energy (b,d) for $15M_{\odot}$ (a, b) and $20M_{\odot}$ (c, d) progenitors. Results are displayed for the positron capture $e^+ + n$ baseline (solid line) together with the predictions of the FT-QRPA neutrinos (dotted line) and antineutrinos (dashed line).

ably, reflecting the rapid increase in EC rates with temperature and density, which drives further deleptonization. We note that this represents the first calculation of average neutrino energy using the FT-QRPA EC rates from Ref. [38], providing a direct comparison between different (anti)neutrino channels with a consistent rate framework.

Conclusions.— In this Letter, we identify the impact of β decays in stellar environments on supernovae dynamics from large-scale, microscopic calculations. The new FT-QRPA calculations span a much larger set of nuclei and produce a significantly enhanced antineutrino spectrum compared to SM calculations, which are mostly limited to pf-shell nuclei. In particular, due to the inclusion of more neutron-rich nuclei, the enhanced antineutrino spectrum, compared to the $e^+ + n$ baseline, extends almost up to $E_{\bar{\nu}_e} = 11$ MeV, primarily because the late-collapse emissivity is dominated by neutron-rich nuclei with $N \approx 50$. When incorporated into CCSNe simulations, the enhanced β decay emissivity translates into a substantially larger ($\sim 10^3$ times) pre-bounce antineutrino luminosity and a slight increase in the average antineutrino energy, while leaving the collapse dynamics unchanged. Nonetheless, the current absence of impact during the collapse dynamics does not imply that β decays are unimportant for stellar evolution, and consequently CCSNe dynamics. Due to β decay's competition with EC at relatively lower densities and temperatures, these new rates have the potential to alter the star's evolution in the presupernova stage, which would in turn modify the initial conditions that shape CCSNe dynamics. A full investigation of these evolutionary effects requires dedicated stellar-evolution calculations and will be pursued in a future work. These results demonstrate that improved nuclear weak-interaction inputs can markedly modify the observable supernova antineutrino signal, providing a realistic pathway for next-generation detectors to probe the final seconds of massive-star evolution.

Data availability.— The β decay rate table used in this work is available from the authors upon request.

Acknowledgements.— Discussions with Remco Zegers, Simon Giraud, Jim Kneller and Kelly Patton are gratefully acknowledged. This work was supported by the U.S. Department of Energy under Award Nos. DOE-DE-NA0004074 (NNSA, the Stewardship Science Academic Alliances program), DE-SC0023688, DE-SC0023128 (Office of Science, Office of Nuclear Physics), and DE-SC0023175 (Office of Science, NUCLEI SciDAC-5 collaboration) and by the Swedish Research Council (Project No. 2020-00452). This work benefited from support in part by the National Science Foundation under Grant No. OISE-1927130 (IReNA). Computational resources were provided in part by the Institute for Cyber-Enabled Research at Michigan State University. This work used TAMU ACES at TAMU through allocation PHY250120

from the Advanced Cyberinfrastructure Coordination Ecosystem: Services & Support (ACCESS) program, which is supported by U.S. National Science Foundation grants No. 2138259, 2138286, 2138307, 2137603, and 2138296.

- * dashertr@msu.edu
- † ravlic@frib.msu.edu
- [‡] lalit@frib.msu.edu
- § evan.oconnor@astro.su.se
- ¶ godbey@frib.msu.edu
- K. Hirata, T. Kajita, M. Koshiba, M. Nakahata, et al., Observation of a neutrino burst from the supernova SN1987A, Phys. Rev. Lett. 58, 1490 (1987).
- [2] R. M. Bionta, G. Blewitt, C. B. Bratton, D. Casper, A. Ciocio, R. Claus, B. Cortez, M. Crouch, S. T. Dye, S. Errede, G. W. Foster, W. Gajewski, K. S. Ganezer, M. Goldhaber, T. J. Haines, T. W. Jones, D. Kielczewska, W. R. Kropp, J. G. Learned, J. M. LoSecco, J. Matthews, R. Miller, M. S. Mudan, H. S. Park, L. R. Price, F. Reines, J. Schultz, S. Seidel, E. Shumard, D. Sinclair, H. W. Sobel, J. L. Stone, L. R. Sulak, R. Svoboda, G. Thornton, J. C. van der Velde, and C. Wuest, Observation of a neutrino burst in coincidence with supernova 1987a in the large magellanic cloud, Phys. Rev. Lett. 58, 1494 (1987).
- [3] E. Alexeyev, L. Alexeyeva, I. Krivosheina, and V. Volchenko, Detection of the neutrino signal from sn 1987a in the lmc using the inr baksan underground scintillation telescope, Physics Letters B 205, 209 (1988).
- [4] J. F. Beacom and M. R. Vagins, Antineutrino spectroscopy with large water Čerenkov detectors, Phys. Rev. Lett. 93, 171101 (2004).
- [5] A. Odrzywolek, M. Misiaszek, and M. Kutschera, Detection possibility of the pair-annihilation neutrinos from the neutrino-cooled pre-supernova star, Astroparticle Physics 21, 303 (2004).
- [6] A. Odrzywolek, M. Misiaszek, and M. Kutschera, Neutrinos from Pre-Supernova Star, Acta Physica Polonica B 35, 1981 (2004), arXiv:astro-ph/0405006 [astro-ph].
- [7] K. Asakura, A. Gando, Y. Gando, T. Hachiya, et al., Kamland sensitivity to neutrinos from pre-supernova stars, The Astrophys. J. 818, 91 (2016).
- [8] H.-K. Proto-Collaboration:, K. Abe, K. Abe, H. Aihara, A. Aimi, et al., Hyper-kamiokande design report (2018), arXiv:1805.04163 [physics.ins-det].
- [9] P. Antonioli, R. T. Fienberg, F. Fleurot, Y. Fukuda, W. Fulgione, A. Habig, J. Heise, A. B. McDonald, C. Mills, T. Namba, L. J. Robinson, K. Scholberg, M. Schwendener, R. W. Sinnott, B. Stacey, Y. Suzuki, R. Tafirout, C. Vigorito, B. Viren, C. Virtue, and A. Zichichi, Snews: the supernova early warning system, New Journal of Physics 6, 114 (2004).
- [10] S. Al Kharusi, S. Y. BenZvi, J. S. Bobowski, W. Bonivento, V. Brdar, T. Brunner, E. Caden, M. Clark, A. Coleiro, M. Colomer-Molla, J. I. Crespo-Anadón, A. Depoian, D. Dornic, V. Fischer, D. Franco, W. Fulgione, A. Gallo Rosso, M. Geske, S. Griswold, M. Gromov, D. Haggard, A. Habig, O. Halim, A. Higuera, R. Hill, S. Horiuchi, K. Ishidoshiro, C. Kato,

- E. Katsavounidis, D. Khaitan, J. P. Kneller, A. Kopec, V. Kulikovskiy, M. Lai, M. Lamoureux, R. F. Lang, H. L. Li, M. Lincetto, C. Lunardini, J. Migenda, D. Milisavljevic, M. E. McCarthy, E. O Connor, E. O Sullivan, G. Pagliaroli, D. Patel, R. Peres, B. W. Pointon, J. Qin, N. Raj, A. Renshaw, A. Roeth, J. Rumleskie, K. Scholberg, A. Sheshukov, T. Sonley, M. Strait, V. Takhistov, I. Tamborra, J. Tseng, C. D. Tunnell, J. Vasel, C. F. Vigorito, B. Viren, C. J. Virtue, J. S. Wang, L. J. Wen, L. Winslow, F. L. H. Wolfs, X. J. Xu, and Y. Xu, Snews 2.0: a next-generation supernova early warning system for multi-messenger astronomy, New Journal of Physics 23, 031201 (2021).
- [11] M. Kara, S. Torres-Lara, A. Baxter-Depoian, S. BenZvi, M. C. Molla, A. Habig, J. P. Kneller, M. Lai, R. F. Lang, M. Linvill, D. Milisavljevic, J. Migenda, C. Orr, K. Scholberg, J. Smolsky, J. Tseng, C. D. Tunnell, J. Vasel, and A. Sheshukov, The snews 2.0 alert software for the coincident detection of neutrinos from core-collapse supernovae (2024), arXiv:2406.17743 [astro-ph.IM].
- [12] J. R. Wilson, J. Centrella, J. LeBlanc, and R. Bowers, Numerical astrophysics, Jones and Bartlett, Boston, 422 (1985).
- [13] K. Langanke, G. Martínez-Pinedo, and R. G. T. Zegers, Electron capture in stars, Reports on Progress in Physics 84, 066301 (2021).
- [14] K. Langanke and G. Martínez-Pinedo, Nuclear weakinteraction processes in stars, Rev. Mod. Phys. 75, 819 (2003).
- [15] T. Suzuki, Nuclear weak rates and nuclear weak processes in stars, Progress in Particle and Nuclear Physics 126, 103974 (2022).
- [16] H.-T. Janka, K. Langanke, A. Marek, G. Martínez-Pinedo, and B. Müller, Theory of core-collapse supernovae, Phys. Rep. 442, 38 (2007), the Hans Bethe Centennial Volume 1906-2006.
- [17] G. Martínez-Pinedo, K. Langanke, and D. J. Dean, Competition of electron capture and beta-decay rates in supernova collapse, The Astrophysical Journal Supplement Series 126, 493 (2000).
- [18] H. A. Bethe, Supernova mechanisms, Rev. Mod. Phys. 62, 801 (1990).
- [19] G. M. Fuller, W. A. Fowler, and M. J. Newman, Stellar weak-interaction rates for sd-shell nuclei. I-Nuclear matrix element systematics with application to Al-26 and selected nuclei of importance to the supernova problem, The Astrophysical Journal Supplement Series 42, 447 (1980).
- [20] G. M. Fuller, W. A. Fowler, and M. J. Newman, Stellar weak interaction rates for intermediate mass nuclei. III-Rate tables for the free nucleons and nuclei with A= 21 to A= 60, The Astrophysical Journal Supplement Series 48, 279 (1982).
- [21] G. M. Fuller, W. A. Fowler, and M. J. Newman, Stellar weak interaction rates for intermediate-mass nuclei. II-A= 21 to A= 60, The Astrophysical Journal 252, 715 (1982).
- [22] G. Fuller, W. Fowler, and M. Newman, Stellar weak interaction rates for intermediate-mass nuclei. IV-Interpolation procedures for rapidly varying lepton capture rates using effective log (ft)-values, The Astrophysical Journal 293, 1 (1985).
- [23] T. Oda, M. Hino, K. Muto, M. Takahara, and K. Sato, Rate tables for the weak processes of sd-shell nuclei in

- stellar matter, Atomic Data and Nuclear Data Tables **56**, 231 (1994).
- [24] K. Langanke and G. Martínez-Pinedo, Supernova electron capture rates on odd-odd nuclei, Physics Letters B 453, 187 (1999).
- [25] K. Langanke and G. Martínez-Pinedo, Shell-model calculations of stellar weak interaction rates: II. Weak rates for nuclei in the mass range A=45-65 in supernovae environments, Nuclear Physics A **673**, 481 (2000).
- [26] S. Zha, S.-C. Leung, T. Suzuki, and K. Nomoto, Evolution of ONeMg core in super-AGB stars toward electron-capture supernovae: Effects of updated electron-capture rate, Astrophys. J. 886, 22 (2019).
- [27] K. M. Patton, C. Lunardini, and R. J. Farmer, Presupernova neutrinos: Realistic emissivities from stellar evolution, The Astrophysical Journal 840, 2 (2017).
- [28] K. M. Patton, C. Lunardini, R. J. Farmer, and F. X. Timmes, Neutrinos from beta processes in a presupernova: Probing the isotopic evolution of a massive star, The Astrophysical Journal 851, 6 (2017).
- [29] A. Heger, K. Langanke, G. Martínez-Pinedo, and S. E. Woosley, Presupernova collapse models with improved weak-interaction rates, Phys. Rev. Lett. 86, 1678 (2001).
- [30] A. Heger, S. E. Woosley, G. Martínez-Pinedo, and K. Langanke, Presupernova evolution with improved rates for weak interactions, The Astrophysical Journal 560, 307 (2001).
- [31] N. Paar, D. Vretenar, E. Khan, and G. Colò, Exotic modes of excitation in atomic nuclei far from stability, Reports on Progress in Physics 70, R02 (2007).
- [32] N. Paar, G. Colò, E. Khan, and D. Vretenar, Calculation of stellar electron-capture cross sections on nuclei based on microscopic skyrme functionals, Phys. Rev. C 80, 055801 (2009).
- [33] A. Ravlić, E. Yüksel, Y. F. Niu, G. Colò, E. Khan, and N. Paar, Stellar electron-capture rates based on finitetemperature relativistic quasiparticle random-phase approximation, Phys. Rev. C 102, 065804 (2020).
- [34] A. A. Dzhioev, A. V. Yudin, N. V. Dunina-Barkovskaya, and A. I. Vdovin, Pre-supernova (anti)neutrino emission due to weak-interaction reactions with hot nuclei, Particles 8, 10.3390/particles8040084 (2025).
- [35] A. A. Dzhioev, A. V. Yudin, N. V. Dunina-Barkovskaya, and A. I. Vdovin, Neutrino Spectrum and Energy Loss Rates Due to Weak Processes on Hot 56Fe in Pre-Supernova Environment, Particles 6, 682 (2023).
- [36] A. A. Dzhioev, A. V. Yudin, N. V. Dunina-Barkovskaya, and A. I. Vdovin, Neutrinos from presupernova in the framework of TQRPA method, Monthly Notices of the Royal Astronomical Society 527, 7701 (2023), https://academic.oup.com/mnras/article-pdf/527/3/7701/54357526/stad3730.pdf.
- [37] A. A. Dzhioev, A. V. Yudin, N. V. Dunina-Barkovskaya, and A. I. Vdovin, Neutrinos from pre-supernova: Effects of nuclear temperature on luminosities and spectra, International Journal of Modern Physics E 33, 2441014 (2024), https://doi.org/10.1142/S0218301324410143.
- [38] A. Ravlić, S. Giraud, N. Paar, and R. G. T. Zegers, Self-consistent microscopic calculations for electron captures on nuclei in core-collapse supernovae, Phys. Rev. C 112, L032801 (2025).
- [39] S. Giraud, R. G. T. Zegers, B. A. Brown, J.-M. Gabler, J. Lesniak, J. Rebenstock, E. M. Ney, J. Engel, A. Ravlić, and N. Paar, Finite-temperature electron-capture rates

- for neutron-rich nuclei near n=50 and effects on core-collapse supernova simulations, Phys. Rev. C **105**, 055801 (2022).
- [40] S. Typel, Relativistic model for nuclear matter and atomic nuclei with momentum-dependent self-energies, Phys. Rev. C 71, 064301 (2005).
- [41] T. Marketin, L. Huther, and G. Martínez-Pinedo, Large-scale evaluation of β -decay rates of r-process nuclei with the inclusion of first-forbidden transitions, Phys. Rev. C 93, 025805 (2016).
- [42] A. Ravlić, E. M. Ney, J. Engel, and N. Paar, Elucidating the finite temperature quasiparticle random phase approximation, The European Physical Journal A 61, 37 (2025).
- [43] E. Yüksel, G. Colò, E. Khan, Y. F. Niu, and K. Bozkurt, Multipole excitations in hot nuclei within the finite temperature quasiparticle random phase approximation framework, Phys. Rev. C 96, 024303 (2017).
- [44] E. Yüksel, N. Paar, G. Colò, E. Khan, and Y. F. Niu, Gamow-teller excitations at finite temperature: Competition between pairing and temperature effects, Phys. Rev. C 101, 044305 (2020).
- [45] A. Ravlić, E. Yüksel, Y. F. Niu, and N. Paar, Evolution of β-decay half-lives in stellar environments, Phys. Rev.

- C **104**, 054318 (2021).
- [46] K. Langanke, G. Martínez-Pinedo, and J. M. Sampaio, Neutrino spectra from stellar electron capture, Phys. Rev. C 64, 055801 (2001).
- [47] K. Langanke and G. Martínez-Pinedo, Rate tables for the weak processes of pf-shell nuclei in stellar environments, Atomic Data and Nuclear Data Tables 79, 1 (2001).
- [48] E. O'Connor, An open-source neutrino radiation hydrodynamics code for core-collapse supernovae, The Astrophysical Journal Supplement Series 219, 24 (2015).
- [49] A. W. Steiner, M. Hempel, and T. Fischer, Core-collapse supernova equations of state based on neutron star observations, The Astrophysical Journal 774, 17 (2013).
- [50] S. E. Woosley and T. A. Weaver, The Evolution and Explosion of Massive Stars. II. Explosive Hydrodynamics and Nucleosynthesis, The Astrophysical Journal Supplement Series 101, 181 (1995).
- [51] Supplemental material (2025), Supplemental Material shows comparisons between electron capture and β -decay rates calculated within our FT-QRPA framework, as well as the comparison between β -decay rates and antineutrino energy loss between our model and the shell-model calculations from Ref. [26]. Contains Refs. [26, 38, 45].

Supplemental Material: Enhanced antineutrino emission from β decay in core-collapse supernovae with self-consistent weak decay rates

T. Dasher , 1,2,* A. Ravlić , 1,3,† S. Lalit , 1, ‡ E. O'Connor , 4, § and K. Godbey , ¶

¹ Facility for Rare Isotope Beams, Michigan State University, East Lansing, Michigan 48824, USA

² Department of Physics and Astronomy, Michigan State University, East Lansing, Michigan 48824, USA

³ Department of Physics, Faculty of Science, University of Zagreb, Bijenička c. 32, 10000 Zagreb, Croatia

¹ The Oskar Klein Centre, Department of Astronomy,

Stockholm University, AlbaNova, SE-106 91 Stockholm, Sweden

(Dated: November 27, 2025)

Supplemental Material shows comparisons between electron capture and β decay rates calculated within our FT-QRPA framework, as well as the comparison between β decay rates and antineutrino energy loss between our model and the shell-model calculations from Ref. [1].

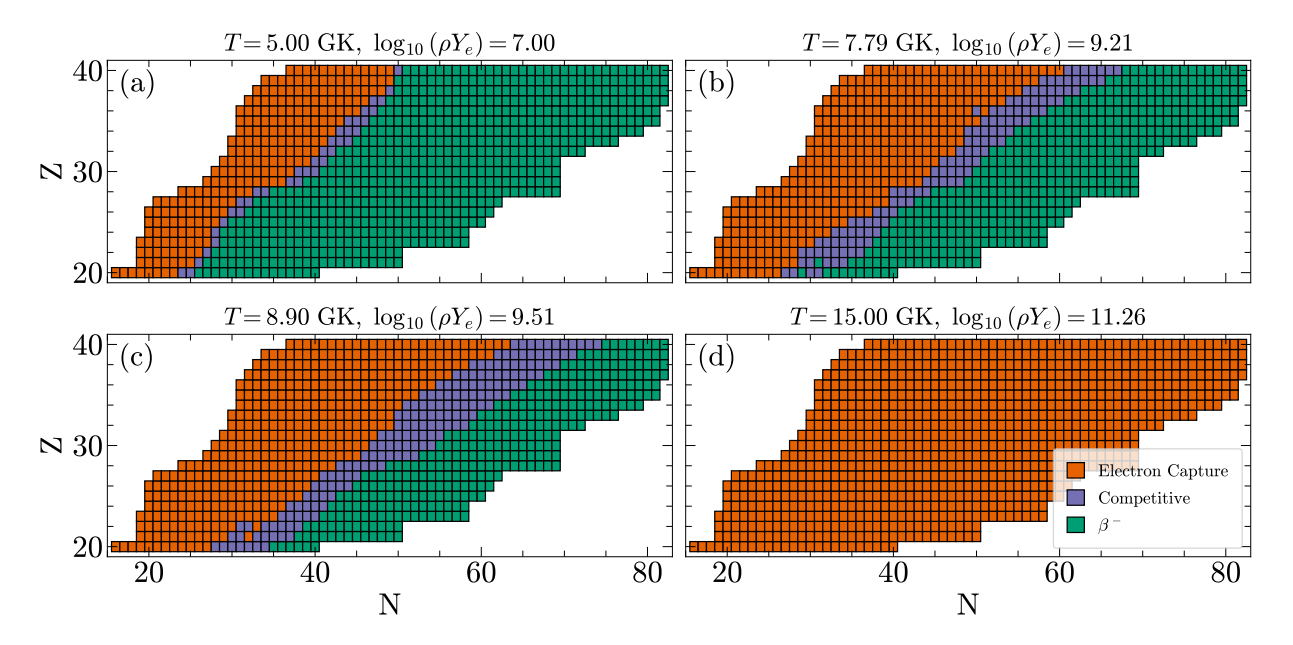


FIG. S1. Competition between EC and β decay rates for representative conditions during the CCSN collapse.

COMPETITION BETWEEN ELECTRON CAPTURE AND β DECAY

Figure S1 shows the regions of the nuclide chart where β decay and electron capture (EC) rates become comparable at representative thermodynamic conditions along the core-collapse supernova (CCSN) trajectory. While the β decay rates are calculated in this work, the EC rates are taken from Ref. [2], obtained within the same theoretical framework. For each nucleus, the two processes are classified as "competitive" when the rates differ by less than one order of magnitude, i.e., $|\log_{10}(\lambda_{\rm EC}/\lambda_{\beta})| \leq 1$. Nuclei with $\lambda_{\rm EC}$ exceeding λ_{β} by more than one order of magnitude are identified as EC dominated, while nuclei with λ_{β} larger than $\lambda_{\rm EC}$ by more than one order of magnitude are labeled as β decay dominated.

The full set of nuclei shown spans $20 \le Z \le 40$ and approximately $16 \le N \le 82$, consistent with the domain of the FT-QRPA rate tables, including 902 individual nuclei. At relatively low temperatures and densities [Fig. S1(a)], β decay dominates much of the domain on the neutron-rich side, with slight competition near the valley of stability. At such low densities, β decays are unhindered by phase-space blocking and dominate in neutron-rich nuclei due to the enhanced Q_{β} window. On the other hand, for proton-rich nuclei, where Q_{β} is low or even negative, EC dominates. In the in-between region, closer to the valley of stability, both rates can compete, though only over a very narrow band. We note that although most of these nuclei would be β -stable at zero temperature, finite-temperature effects can unblock the β decay rates. As temperature and density increase during collapse [Figs. S1(b)-(d)], the competitive

band shifts to more neutron-rich nuclei and broadens toward the neutron-rich region, reflecting the fact that EC rates start increasing rapidly at higher temperatures and densities, while the β decay phase-space gets Pauli blocked as the density is increased. Finally, in Fig. S1(d), as the collapse progresses to hotter, more dense conditions, EC dominates fully.

We also note that the competitive regions identified in Fig. S1 partially coincide with the nuclei that contribute most strongly to the antineutrino emissivity shown in Fig. 2 of the main text. Although the thermodynamic conditions are not identical, they lie along the same CCSN trajectory and probe similar density–temperature regimes. In particular, comparison with the emissivity patterns at comparable thermodynamic points demonstrates that the nuclei classified here as competitive, and often β decay dominated, have a significant impact on the antineutrino emissivity at $E_{\bar{\nu}_e} = 3$ MeV and 8 MeV. This is especially the case for nuclei around the N = 50 region.

COMPARISON OF FT-QRPA AND SHELL-MODEL β DECAY RATES

Figure S2 compares the β decay rates obtained in this work with available shell-model calculations from Ref. [1] by showing the logarithmic ratio $\log_{10}(\lambda_{\text{FT-QRPA}}/\lambda_{\text{SM}})$ along the CCSN trajectory. Only nuclei for which both sets of rates exist are included, restricting the comparison primarily to the pf-shell region with $20 \le Z \le 30$ and $22 \le N \le 38$.

Across all representative thermodynamic conditions shown, FT-QRPA rates are typically higher than shell-model values, even up to 3 orders of magnitude. This is consistent with the observations in Ref. [3] for β decay rates obtained within a similar theoretical framework, as well as for the EC in Ref. [2]. Considering the fact that for pf-shell nuclei, the strength is mostly dominated by the allowed transitions, first-forbidden being negligible, as a possible reason for the observed differences, we note that considerable β -strength in the FT-QRPA originates from de-excitations, *i.e.* transitions from the highly-excited states in the parent nucleus. These systematic differences are consistent with the behavior discussed in the main text and persist across all thermodynamic points sampled along the core-collapse trajectory.

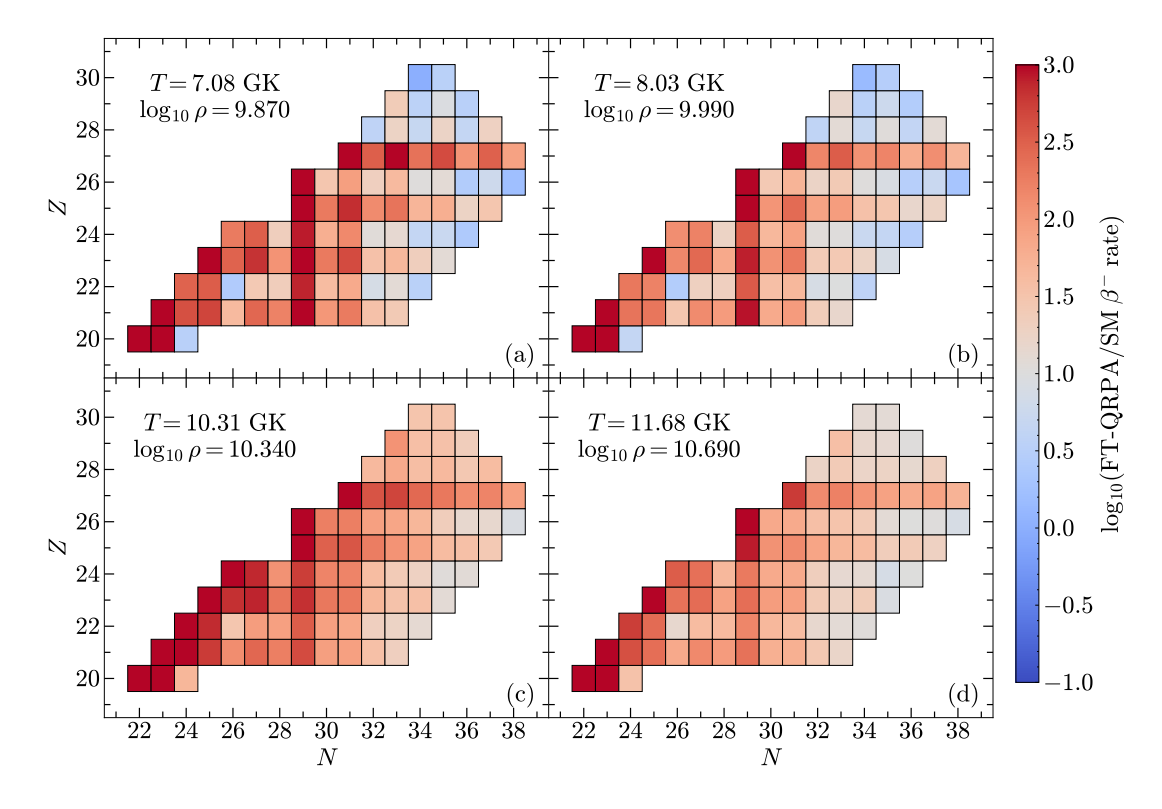


FIG. S2. Comparison between our FT-QRPA and shell-model rates [1] at representative points along the CCSNe trajectory.

COMPARISON OF FT-QRPA AND SHELL-MODEL ANTINEUTRINO ENERGY LOSS RATES

Figure S3 shows the logarithmic ratio of antineutrino energy loss rates (defined in Eq. 2 of the main paper) obtained with the FT-QRPA and shell-model β decay calculations at representative points along the CCSN trajectory. As in Fig. S2, only nuclei for which both sets of rates are available are included.

The plotted quantity highlights differences in the total antineutrino energy loss rate originating from individual nuclei. Because energy loss rates inherit the β decay rate differences and variations of the underlying antineutrino spectral distribution $n(E_{\bar{\nu}_e})$ scale proportionally, the magnitude and sign of the deviations generally mirror the patterns observed in Fig. S2.

Across all thermodynamic conditions considered, FT-QRPA energy loss rates are typically higher than shell-model predictions in the region where both models overlap.

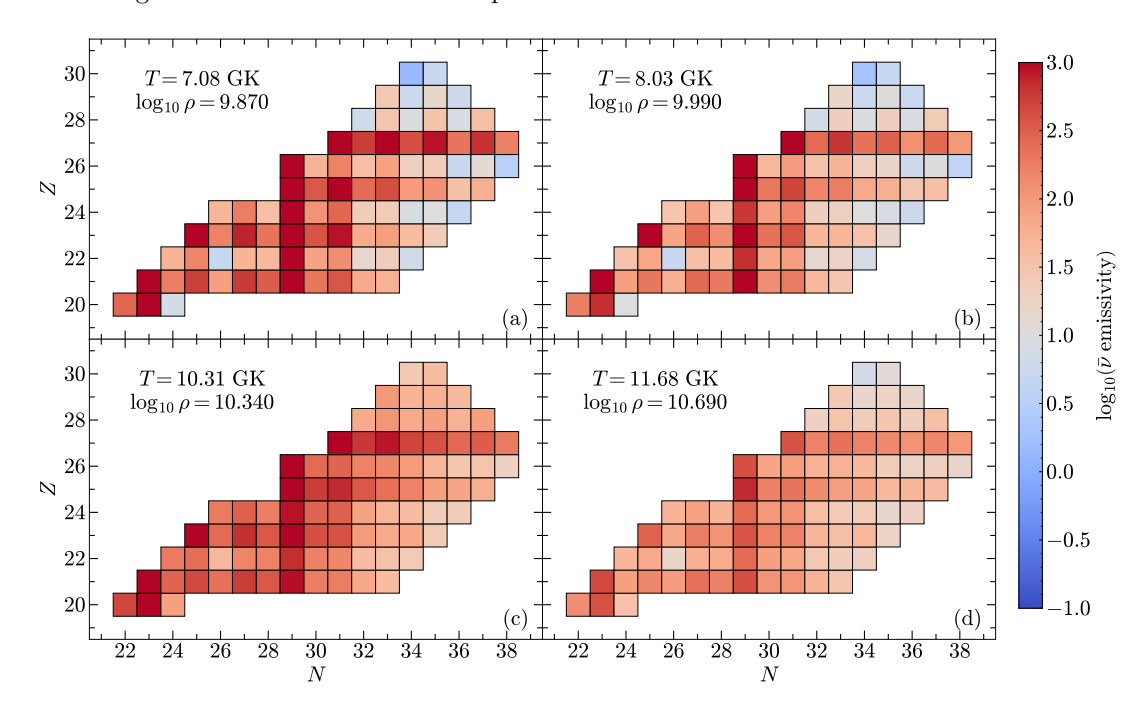


FIG. S3. Same as in Fig. S2, but for antineutrino energy loss.

^{*} dashertr@msu.edu

[†] ravlic@frib.msu.edu

[‡] lalit@frib.msu.edu

[§] evan.oconnor@astro.su.se

[¶] godbey@frib.msu.edu

^[1] S. Zha, S.-C. Leung, T. Suzuki, and K. Nomoto, Evolution of ONeMg core in super-AGB stars toward electron-capture supernovae: Effects of updated electron-capture rate, Astrophys. J. 886, 22 (2019).

^[2] A. Ravlić, S. Giraud, N. Paar, and R. G. T. Zegers, Self-consistent microscopic calculations for electron captures on nuclei in core-collapse supernovae, Phys. Rev. C 112, L032801 (2025).

^[3] A. Ravlić, E. Yüksel, Y. F. Niu, and N. Paar, Evolution of β -decay half-lives in stellar environments, Phys. Rev. C **104**, 054318 (2021).